The Unique Characteristics of ON and OFF Retinal Ganglion Cells: A Modeling Study

Tianruo Guo, *Student Member, IEEE,* David Tsai, *Member, IEEE,* John W. Morley, Gregg J. Suaning, *Senior Member, IEEE*, Nigel H. Lovell, *Fellow, IEEE* and Socrates Dokos, *Member, IEEE*

***Abstract*—Retinal ganglion cells (RGCs) demonstrate a large range of variation in their ionic channel properties and morphologies. These cell-specific properties are responsible for the unique way they process synaptic inputs. A cell-specific modeling approach allows us to examine the functional significance of regional membrane channel expression and cell morphology. ON and OFF RGC models based on accurate biophysics and realistic representation of morphologies were used to study the contribution of different ion channel properties and spatial structure of neurons to RGC electrical activity. Using this approach, morphologically-complex retinal neurons such as amacrine cells or RGCs can be modelled and their interactions and processing can be better understood.**

I. Introduction

Despite the successful identification and quantitative defining of functional significance of photoreceptors, horizontal and bipolar cells in mammalian retina (for a review refer to [1]), the detailed mechanisms underlying the responses of morphologically-complex retinal neurons such as amacrine cells or retinal ganglion cells (RGCs) are still not clear. There are ~13 identified amacrine cell types and ~20 RGCs types. A definitive description of these cells has not been made yet due to their rich diversity in both intrinsic and physical properties. Limited experimental information on ionic channel kinetics and distribution in identified cell types also makes cell-specific study a difficult task.

Over the past several decades, a large number of biophysically-detailed models were developed to understand the underlying ionic mechanisms in RGC electrophysiology. These models have led to a quantitative understanding of many dynamical phenomena in the RGCs, including spike frequency adaptation [2], rebound activities [3, 4], burst firing [4], sub-threshold activities [4], action potential (AP) initiation [5], dendritic processing [6], as well as the effect of extracellular stimuli [7], temperature [8] and cell morphology [9]. However, existing ionic models of RGCs have been largely limited to identification of individual RGC types without considering the functional significance of regional membrane channel distributions/kinetics and complex morphology. Moreover, no work has been reported on the large-scale parameter optimization to simultaneously fit multiple datasets under different experimental conditions. In addition, the ability of existing models to predict the experimental information is still unclear.

In this study, we have used a realistic modeling approach to study the cell-specific biophysical and physical mechanisms underlying ON and OFF RGC types. Our models were optimized to simultaneously reconstruct multiple biological RGC responses with high accuracy, and to closely predict other published experimental information.

T. Guo, D. Tsai, G. J. Suaning, N. H. Lovell and S. Dokos are with the Graduate School of Biomedical Engineering, University of New South Wales, Sydney, 2052, Australia. D. Tsai is also with the Howard Hughes Medical Institute, Biological Sciences, Columbia University, New York, NY, USA and Bioelectronic Systems Lab, Electrical Engineering, Columbia University, New York, NY, USA. J. W. Morley is with School of Medicine, University of Western Sydney, Australia.

E-mail for correspondence: t.guo@unsw.edu.au

II. Methodology

A. Biophysically-detailed ON and OFF RGC models

The RGC electrophysiology can be modelled by the equivalent cable equation:

$$\sigma \frac{\partial^2 V_m}{\partial x^2} = A\left(C_m \frac{dV_m}{dt} + J_{ion}\right) \quad (1)$$

where V_m represents membrane potential, x is the axial cable distance, σ is the intracellular conductivity (mS·cm^{-1}), A is the local cell surface to volume ratio (cm^{-1}), C_m is membrane capacitance per unit membrane area. J_{ion} (μA·cm-2) represents the ionic currents, consisting of seven time-dependent currents and one leakage current. The ON and OFF RGC models were simultaneously fit to multiple (at different hyper- and depolarizations) time-series AP datasets and 2-D phase plot (AP waveform) datasets recorded from each cell type. Parameter values were estimated using a custom curvilinear gradient-based optimization method [10]. Detailed ionic current formulations and parameter values can be found in Tables I-III.

B. ON and OFF cell morphology reconstruction

One ON cell with ~251 μm average dendritic diameter, at a depth of ~40% (the edge of the ganglion cell layer being 0%) into the inner plexiform layer (IPL), one OFF Parasol cell with ~208 μm average dendritic diameter, at a depth of ~90% into the IPL were identified in rabbit retinae. Morphological data were digitized and imported into NEURON 7.2 [11], which approximated the cable equation (1) into a multi-compartmental representation of the neuron, equivalent to a finite-difference approximation of the spatial second derivative. We included in the model representations of soma, axon initial segment (AIS), axon hillock, axon and dendrites. More than 1000 morphological segments were chosen to ensure the accurate spatial granularity.

978-1-4244-7929-0/14/$26.00 ©2014 IEEE

III. RESULTS

A. ON and OFF RGC response patterns

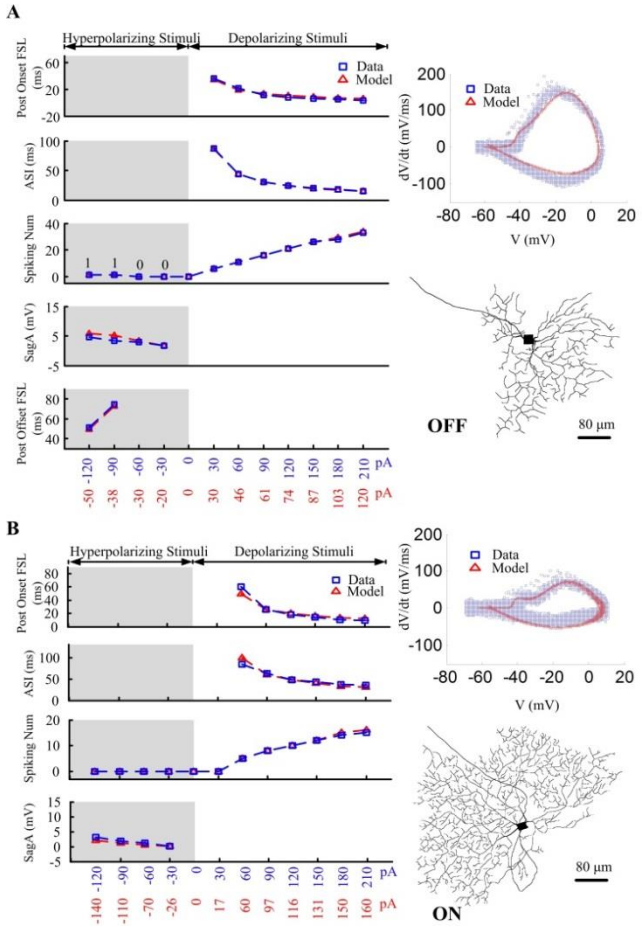

Fig. 1 Simulated (red) and experimental (blue) ON and OFF somatic spiking patterns under multiple intracellular current injection conditions. A. Left: The OFF RGC model was optimized to reconstruct post onset first spike latency, averaged spiking interval (ASI), spiking number, sag amplitude and post offset first spike latency (FSL). Right: AP waveform phase plot and reconstructed cell morphology. B. Simulated responses patterns using model ON RGC. Note that ON RGC does not demonstrate rebound activities.

Model ON and OFF cells exhibited unique spiking patterns and firing property variations caused by different stimulus amplitudes (see Fig. 1). The model ON cell demonstrated less excitability, lower spiking latency, and lower 'sag' amplitude in response to hyperpolarizing injections compared to the model OFF cell. In addition, the ON model did not exhibit any rebound excitation in response to hyperpolarizing injections. Besides multiple spiking patterns, the rate of membrane voltage change also differed between the two model neurons. In particular, the model ON cell exhibited lower rates of rising/falling phases, higher overshoot and more obvious initial segment-soma dendritic (IS-SD) break than the OFF cell. All of these simulation results closely matched the experimental recordings from biological RGCs. The results of experimental (blue) and simulated (red) somatic current injection for ON and OFF cell were shown in Fig. 1.

ON and OFF RGC models also exhibited significantly different ionic channel distributions (Table 1) which contributed to the cell-specific AP firing patterns in response to multiple somatic injections. Particularly, when examining the I_{Na} ratio for the AIS compared with the soma, the ON cell demonstrated a value of approximately seven compared with a value of four in the OFF cell. Moreover, higher dendritic I_h (twofold to that in soma) and I_{CaT} density (fivefold to that in soma) were set in the OFF cell, compared to a relatively low I_h (1.3 times greater than in the soma) and I_{CaT} (equal to that of the soma) in the ON cell model.

B. Electrical activity in different RGC regions

We also recorded the membrane potential of each model at the AIS, soma and distal dendrite (Fig. 2), while stimulating at the soma. Different dendritic AP waveforms and amplitudes were observed between ON and OFF RGC models. Through dendritic data were not used during model optimization, our model-reconstructed active dendritic responses were close to the recent dendritic recordings reported in RGCs [12] .

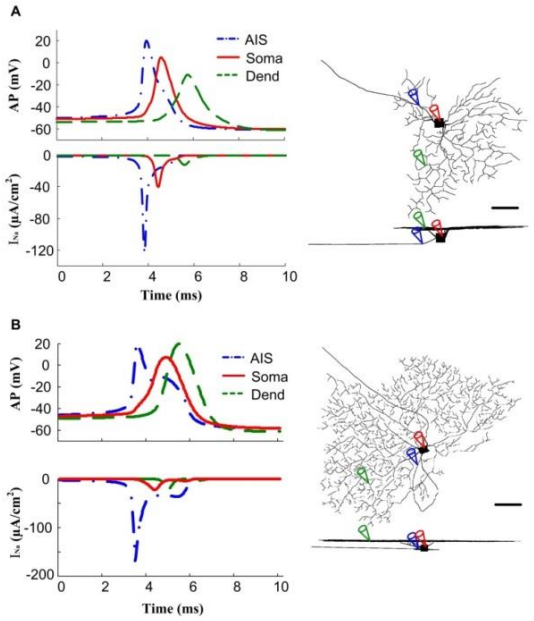

Fig. 2. Cell-specific full AP in dendrites and high sodium channel density in the axon initial segment. A. Upper: Model-reconstructed AP in axon initial segment (blue), soma (red) and dendritic tree (green) using model OFF RGC. Lower: Model-reconstructed Na^+ current from axon initial segment (blue), soma (red) and dendritic tree (green). Right. Location of AIS, somatic and dendritic recording in OFF cell morphology. B. Model-reconstructed AP and Na^+ current using model ON RGC. Scale bar: 80 μm.

IV. DISCUSSION

In this study, the channel distribution and kinetic parameters that were used after model optimization are fully dependent on what our multiple datasets suggested. Importantly, we note that the resulting model parameters are all supported by relevant experimental evidence: 1) the presence of rebound activity is related to higher I_h and I_{CaT} somato-dendritic ratio

TABLE I. IONIC CHANNEL DISTRIBUTIONS IN ON AND OFF RGC MODEL

Channel	Regional maximum membrane conductances (mS/cm^2)										
	Soma	**Axon**	**AIS**	**Hillock**	**Dendrites**		**Soma**	**Axon**	**AIS**	**Hillock**	**Dendrites**
OFF						**ON**					
I_{Na}	68.4	68.4	249	68.4	21.68	I_{Na}	147.3	147.3	1072	147.3	105.526
I_K	45.9	45.9	68.85	45.9	42.83	I_K	16.2	16.2	40.5	16.2	7.559
I_{KA}	18.9	-	18.9	18.9	13.86	I_{KA}	37.8	-	94.5	37.8	27.7187
I_{Ca}	1.6	-	1.6	1.6	2.133	I_{Ca}	2.1	-	2.1	2.1	2.7999
I_{KCa}	0.0474	0.0474	0.0474	0.0474	7.3e-4	I_{KCa}	0.04	0.04	0.04	0.04	6.1e-4
I_h	0.1429	0.1429	0.1429	0.1429	0.286	I_h	0.4287	0.4287	0.4287	0.4287	0.5573
I_{CaT}	0.1983	0.1983	0.1983	0.1983	0.992	I_{CaT}	0.008	0.008	0.008	0.008	0.008
I_L	0.0339	0.0339	0.0339	0.0339	0.0363	I_L	0.0206	0.0206	0.0206	0.0206	0.0305

TABLE II. KINETIC PARAMETERS FOR OFF RGC MODEL

Channel	**Ionic current formulations and rate functions**	
I_{Na}	$I_{Na} = \bar{g}_{Na} m^3 h (V_m - 35)$	
	$\alpha_m = -0.6(V_m + 30)/(e^{-0.1(V_m+30)} - 1)$	$\beta_m = 20e^{-(V_m+55)/18}$
	$\alpha_h = 0.4e^{-(V_m+50)/20}$	$\beta_h = 6/(1 + e^{-0.1(V_m+20)})$
I_{Ca}	$I_{Ca} = \bar{g}_{Ca} c^3 (V_m - V_{Ca})$	
	$\frac{d[Ca^{2+}]_i}{dt} = -(1.5 I_{Ca}) - \frac{[Ca^{2+}]_i - 0.0001}{55}$	$V_{Ca} = 13.2 \ln(\frac{1.8}{[Ca^{2+}]_i})$
	$\alpha_c = -0.15(V_m + 13)/(e^{-0.1(V_m+13)} - 1)$	$\beta_c = 10e^{-(V_m+38)/18}$
I_K	$I_K = \bar{g}_K n^4 (V_m + 68)$	
	$\alpha_n = -0.02(V_m + 40)/(e^{-0.1(V_m+40)} - 1)$	$\beta_n = 0.4e^{-(V_m+50)/80}$
I_{KA}	$I_{KA} = \bar{g}_{KA} A^3 h_A (V_m + 68)$	
	$\alpha_A = -0.003(V_m + 90)/(e^{-0.1(V_m+90)} - 1)$	$\beta_A = 0.1e^{-(V_m+30)/10}$
	$\beta_{hA} = 0.04e^{-(V_m+70)/20}$	$\beta_{hA} = 0.6/(1 + e^{-0.1(V_m+40)})$
I_{KCa}	$I_{KCa} = \bar{g}_{KCa}(V_m + 68)$	
	$g_{KCa} = \bar{g}_{KCa}[(\frac{[Ca^{2+}]_i}{0.001})^2/(1 + (\frac{[Ca^{2+}]_i}{0.001})^2)]$	
I_h	$I_h = \bar{g}_{Na}\, y\, (V_m + 26.8)$	
	$y_\infty = 1/(1 + e^{(V+75)/5.5})$	$\tau_h = 588.2\, e^{0.01(V_m+10)}/(1 + e^{0.2(V_m+10)})$
I_{CaT}	$I_{CaT} = \bar{g}_{Na}\, m_T{}^3 h_T\, (V_m - V_{Ca})$	
	$\alpha_{mT} = 1/(1.7 + \mathrm{e}^{-(V_m+28.8)/13.5})$	$\beta_{mT} = \left(1 + \mathrm{e}^{-\frac{V_m+63}{7.8}}\right)/(1.7 + \mathrm{e}^{-\frac{V_m+28.8}{13.5}})$
	$\alpha_{hT} = \mathrm{e}^{-(V_m+160.3)/17.8}$	$\beta_{hT} = \alpha_{hT}(\sqrt{0.25 + \mathrm{e}^{\frac{V_m+83.5}{6.3}}} - 0.5)$
	$\alpha_d = (1 + \mathrm{e}^{\frac{V_m+37.4}{30}})/(240(0.5 + \sqrt{0.25 + e^{\frac{V_m+83.5}{6.3}}}))$	$\beta_d = \alpha_d \sqrt{0.25 + \mathrm{e}^{\frac{(V_m+83.5)}{6.3}}}$
I_L	$I_L = \bar{g}_L(V_m + 70.5)$	

in the OFF cell model compared to that of the ON cell model. Recent experimental evidence in RGCs also suggested the presence of higher I_{CaT} density in dendrites [13]. Despite the limited experimental information on I_h distribution in RGCs, this current was found to have higher density in CA1 pyramidal neuron dendrites [14]. 2) a large range of threshold variations and the difference in the IS-SD break in 2-D phase plots between ON and OFF cells can be explained by their unique Na^+ kinetics and regional distribution between the two models. It should be noted that I_{Na} was reported to demonstrate appreciably different kinetics among different RGC types [15, 16]. Although the AP waveforms (2-D phase plot) were considered secondary compared with spiking patterns in neuronal identification [17, 18], we found the unique AP waveforms among RGC types can be an effective indicator of cell-specific ionic channel distributions. 3) our ON and OFF RGC models also demonstrated the different I_h kinetics, as suggested by their unique depolarizing sag waveform. This is supported in the literature as different neuronal types [14, 19] including RGCs [20] were found to demonstrate variable kinetics of I_h activation and inactivation.

TABLE III.
SPECIFIC KINETIC PARAMETERS FOR ON RGC MODEL

Channel	Rate functions
I_{Na}	$\alpha_m = -0.3041(V_m + 30)/(e^{-0.1(V_m+30)} - 1)$
I_{Ca}	$\frac{d[Ca^{2+}]_i}{dt} = -(1.5I_{Ca}) - \frac{[Ca^{2+}]_i - 0.0001}{13.75}$
I_K	$I_K = \bar{g}_K n^4 (V_m + 72)$
I_{KA}	$I_{KA} = \bar{g}_{KA} A^3 h_A (V_m + 72)$
	$\alpha_{hA} = 0.002e^{-(V_m+70)/20}$ $\beta_{hA} = 0.03/(1 + e^{-0.1(V_m+40)})$
I_{KCa}	$I_{KCa} = \bar{g}_{KCa}(V_m + 72)$
I_h	$I_h = \bar{g}_{Na}\, y\, (V_m + 45.8)$
	$\tau_h = 4649\, e^{0.01(V_m+20)}/(1 + e^{0.2(V_m+20)})$
I_L	$I_L = \bar{g}_L(V_m + 66.5)$

Table III. Specific kinetic parameters for the model ON RGC. All other parameter values are shared with the model OFF RGC

Morphologically-realistic modelling can be used to study how the APs propagate through the complex RGC structure following intracellular stimulation. Since it is difficult to measure dendritic activities using current patch-clamp techniques, we can only find limited experimental evidence of full dendritic APs [12]. Our optimized models can closely reconstruct published dendritic AP waveforms. This model's potential can be further validated using other 'non-optimized' experimental information including patch-clamp recording in different RGC regions and RGC responses to different types of extracellular electrical stimulations.

ACKNOWLEDGMENT

This research was supported by the Australian Research Council (ARC) through a Special Research Initiative in Bionic Vision Science and Technology grant to Bionic Vision Australia (BVA).

REFERENCES

[1] R. H. Masland, "The neuronal organization of the retina," *Neuron,* vol. 76, pp. 266-80, 2012.
[2] J. F. Fohlmeister and R. F. Miller, "Impulse encoding mechanisms of ganglion cells in the tiger salamander retina," *J Neurophysiol,* vol. 78, pp. 1935-1947, 1997.
[3] T. Guo, D. Tsai, G. J. Suaning, N. H. Lovell, and S. Dokos, "Modeling normal and rebound excitation in mammalian retinal ganglion cells," *Conf Proc IEEE Eng Med Biol Soc,* vol. 2012, pp. 5506-9, 2012.
[4] T. Kameneva, H. Meffin, and A. N. Burkitt, "Modelling intrinsic electrophysiological properties of ON and OFF retinal ganglion cells," *J Comput Neurosci,* vol. 31, pp. 547-561, 2011.
[5] J. Jeng, S. Tang, A. Molnar, N. J. Desai, and S. I. Fried, "The sodium channel band shapes the response to electric stimulation in retinal ganglion cells," *J Neural Eng,* vol. 8, p. 036022, 2011.
[6] M. J. Schachter, N. Oesch, R. G. Smith, and W. R. Taylor, "Dendritic spikes amplify the synaptic signal to enhance detection of motion in a simulation of the direction-selective ganglion cell," *PLoS Comput Biol,* vol. 6, 2010.
[7] D. Tsai, S. Chen, D. A. Protti, J. W. Morley, G. J. Suaning, and N. H. Lovell, "Responses of retinal ganglion cells to extracellular electrical stimulation, from single cell to population: model-based analysis," *PLoS One,* vol. 7, p. e53357, 2012.
[8] J. F. Fohlmeister, E. D. Cohen, and E. A. Newman, "Mechanisms and distribution of ion channels in retinal ganglion cells: using temperature as an independent variable," *J Neurophysiol,* vol. 103, pp. 1357-1374, 2010.
[9] M. I. Maturana, T. Kameneva, A. N. Burkitt, H. Meffin, and D. B. Grayden, "The effect of morphology upon electrophysiological responses of retinal ganglion cells: simulation results," *J Comput Neurosci,* 2013.
[10] S. Dokos and N. H. Lovell, "Parameter estimation in cardiac ionic models," *Prog Biophys Mol Biol,* vol. 85, pp. 407-431, 2004.
[11] M. L. Hines and N. T. Carnevale, "The NEURON simulation environment," *Neural Computation,* vol. 9, pp. 1179-1209, 1997.
[12] B. Sivyer and S. R. Williams, "Direction selectivity is computed by active dendritic integration in retinal ganglion cells," *Nat Neurosci,* vol. 16, pp. 1848-1856, 2013.
[13] R. F. Miller, K. Stenback, D. Henderson, and M. Sikora, "How voltage-gated ion channels alter the functional properties of ganglion and amacrine cell dendrites," *Arch Ital Biol,* vol. 140, pp. 347-359, 2002.
[14] J. C. Magee, "Dendritic hyperpolarization-activated currents modify the integrative properties of hippocampal CA1 pyramidal neurons," *J Neurosci,* vol. 18, pp. 7613-7624, 1998.
[15] M. Kaneda and A. Kaneko, "Voltage-gated sodium currents in isolated retinal ganglion cells of the cat: relation between the inactivation kinetics and the cell type," *Neurosci Res,* vol. 11, pp. 261-75, 1991.
[16] S. A. Lipton and D. L. Tauck, "Voltage-dependent conductances of solitary ganglion cells dissociated from the rat retina," *J Physiol,* vol. 385, pp. 361-91, 1987.
[17] B. J. O'Brien, T. Isayama, R. Richardson, and D. M. Berson, "Intrinsic physiological properties of cat retinal ganglion cells," *J Physiol,* vol. 538, pp. 787-802, 2002.
[18] R. C. Wong, S. L. Cloherty, M. R. Ibbotson, and B. J. O'Brien, "Intrinsic physiological properties of rat retinal ganglion cells with a comparative analysis," *J Neurophysiol,* vol. 108, pp. 2008-2023, 2012.
[19] H. C. Pape, "Queer current and pacemaker: the hyperpolarization-activated cation current in neurons," *Annu Rev Physiol,* vol. 58, pp. 299-327, 1996.
[20] S. C. Lee and A. T. Ishida, "I-h without K-ir in adult rat retinal ganglion cells," *Journal of Neurophysiology,* vol. 97, pp. 3790-3799, 2007.